

Is there a connection between Broad Absorption Line Quasars and Narrow Line Seyfert 1 galaxies?

Dirk Grupe^{1,2}, John.A. Nousek²

ABSTRACT

We consider whether Broad Absorption Line Quasars (BAL QSOs) and Narrow Line Seyfert 1 galaxies (NLS1s) are similar, as suggested by Brandt & Gallagher (2000) and Boroson (2002). For this purpose we constructed a sample of 11 BAL QSOs from existing Chandra and Swift observations. We found that BAL QSOs and NLS1s both operate at high Eddington ratios L/L_{Edd} , although BAL QSOs have slightly lower L/L_{Edd} . BAL QSOs and NLS1s in general have high $\text{FeII}/\text{H}\beta$ and low $[\text{OIII}]/\text{H}\beta$ ratios following the classic 'Boroson & Green' eigenvector 1 relation. We also found that the mass accretion rates \dot{M} of BAL QSOs and NLS1s are more similar than previously thought, although some BAL QSOs exhibit extreme mass accretion rates of more than $10 M_{\odot}/\text{year}$. These extreme mass accretion rates may suggest that the black holes in BAL QSOs are relativistically spinning. Black hole masses in BAL QSOs are a factor of 100 larger than NLS1s. From their location on a M - σ plot, we find that BAL QSOs contain fully developed black holes. Applying a principal component analysis to our sample we find eigenvector 1 to correspond to the Eddington ratio L/L_{Edd} , and eigenvector 2 to black hole mass.

Subject headings: galaxies: active

1. Introduction

Outflows are a ubiquitous property of AGN. For example, blue-shifted emission lines like $[\text{OIII}]\lambda 5007$ (e.g., Zhang et al. 2011; Komossa et al. 2008a), or blue shifted absorption lines in the UV or X-rays (e.g., Crenshaw et al. 2004) are typically interpreted as signs of outflowing gas. Outflows can be driven in principle magnetically, thermally, and through radiation (e.g., Kurasawa & Proga 2009a,b; Proga & Kallman 2004). Because of the large kinetic energy and angular momentum transport outwards, outflows have strong influences on the AGN environment. As a consequence, many AGN parameters are driven by the Eddington ratio L/L_{Edd} (e.g., Boroson 2002; Sulentic et al. 2000; Grupe 2004; Xu et al. 2012). The class of AGN that shows

the strongest outflows as defined by largest absorption column density and outflow velocity (besides jets) are Broad Absorption Line Quasars (BAL QSOs, e.g., Weymann et al. 1991) which can reach outflow velocities of more than 20000 km s^{-1} (e.g., Hamann et al. 2008). Roughly 10-20% of optically-selected quasars belong to this class (e.g., Dai et al. 2008; Elvis 2000) with even higher percentage among infrared selected samples. However, it has also been suggested that the occurrence of BALs may mark a specific time in the life of a quasar (Mathur 2000; Becker et al. 2000). Because the strength of radiation driven outflow directly depends on L/L_{Edd} , we infer that BAL QSOs have extreme values for L/L_{Edd} (e.g., Boroson 2002).

In the local Universe the AGN with the highest L/L_{Edd} are Narrow Line Seyfert 1 galaxies (NLS1s; Osterbrock & Pogge 1985), which are historically defined as Seyfert 1s with a $\text{FWHM}(\text{H}\beta) < 2000 \text{ km s}^{-1}$ and $[\text{OIII}]/\text{H}\beta < 3$ (Goodrich 1989). Although this is a rather crude definition (see for example Zamfir et al. 2009;

¹Space Science Center, Morehead State University, 235 Martindale Dr., Morehead, KY 40351; d.grupe@moreheadstate.edu

²Department of Astronomy and Astrophysics, Pennsylvania State University, 525 Davey Lab, University Park, PA 16802

Marziani et al. 2009), for the purpose of our study we adopt this definition throughout the paper. NLS1s have drawn a lot of attention over the last two decades due to their extreme properties, such as, on average, steep X-ray spectra, strong Fe II emission and weak emission from the Narrow Line Region (e.g., Boroson & Green 1992; Grupe 2004; Komossa 2008). All these properties are linked, and are most likely driven primarily by the mass of the central black hole and the Eddington ratio L/L_{Edd} . Generally speaking, NLS1s are AGN with low black hole masses and high L/L_{Edd} . NLS1s have also been considered to be AGN in an early stage of their evolution (Grupe et al. 1999; Mathur 2000).

It has been suggested by Brandt & Gallagher (2000) and Boroson (2002) that BAL QSOs and NLS1s are similar with respect to their high L/L_{Edd} . It has also been found that the rest-frame optical spectra of at least some BAL QSOs look very much like low-redshift NLS1s (e.g., Marziani et al. 2009; Dietrich et al. 2009). As pointed out by Boroson (2002), BAL QSOs and NLS1s have very similar $\text{FeII}/\text{H}\beta$ and $[\text{OIII}]/\text{H}\beta$ ratios and follow the classical 'Boroson & Green (1992) eigenvector 1' relation. This is remarkable, because BAL QSOs and NLS1s differ in their black hole masses and appear to be at opposite ends of the M_{BH} spectrum. Typically Seyfert 1s with large black hole masses have larger $[\text{OIII}]/\text{H}\beta$ and smaller $\text{FeII}/\text{H}\beta$ ratios than NLS1s (or BAL QSOs) as shown for example in Grupe (2004) and Grupe et al. (2010). Although there seem to be many similarities between NLS1s and BAL QSOs, as pointed out by Laor & Brandt (2002), the strengths of the broad absorption lines (BALs) seem to be directly correlated with the luminosity of the AGN and BALs appear only in highly-luminous AGN.

So far only one object has been established that shows a clear connection between NLS1s and BAL QSO: the X-ray transient NLS1 WPVS 007 (e.g. Grupe et al. 2013). This NLS1s was discovered as a bright X-ray AGN during the ROSAT All-Sky Survey (RASS, Voges et al. 1999), but showed a dramatic drop in its X-ray flux when observed a few years later (Grupe et al. 1995). Various follow-up observations by ROSAT, Chandra, XMM and *Swift* all confirmed this X-ray low state (Grupe et al. 2008b; Grupe et al. 2013,

and references therein). The X-ray spectra of WPVS 007 can be modeled by a power law with a strong partial covering absorber in the line of sight (Grupe et al. 2008b; Grupe et al. 2013). UV spectroscopy by FUSE and HST revealed that strong broad absorption line features had evolved within just a decade (Leighly et al. 2009; Cooper et al. 2013, and Cooper et al. 2014, in prep).

Another NLS1 suggested to be a link between NLS1s and BAL QSOs is Mkn 335 which was discovered by *Swift* in May 2007 to be in a deep X-ray flux state (Grupe et al. 2007b). Although the X-ray data of Mkn 335 can be modeled by a partial covering absorber (Grupe et al. 2008a, 2012) they can also be fitted by reflection models (Grupe et al. 2008a; Gallo et al. 2013). Nevertheless, Mkn 335 has also developed UV absorption lines as reported by (Longinotti et al. 2013). This new finding may suggest that Mkn 335 will develop similar UV absorption lines as WPVS 007 did over the last two decades.

Although BAL QSOs were considered not to be variable, more recent studies have shown that BAL QSOs indeed show variability not only in their UV absorption lines (Filiz Ak et al. 2012, 2013; Hamann et al. 2008; Capellupo et al. 2011, 2012, e.g.), also in X-rays as reported by Saez et al. (2012). On the other hand, NLS1s are known to be highly variable in X-rays (e.g. Grupe et al. 2001, 2010).

The goal of this paper is to search for similarities in the spectral energy distributions and emission line properties of BAL QSOs and NLS1s. The motivation is to test if NLS1s and BAL QSOs are both high L/L_{Edd} AGN but appear to have different distributions of their black hole masses and mass accretion rates, as suggested by Brandt & Gallagher (2000) and Boroson (2002). The outline of this paper is as follows: in § 2 we describe sample selection and the observations and data reduction by *Swift* and *Chandra*, as well as in the infrared and in the optical. In § 3 we present the results from the analysis of the spectral energy distributions. In § 4 we discuss the results. Throughout the paper spectral indices are denoted as energy spectral indices with $F_\nu \propto \nu^{-\alpha}$. Luminosities are calculated assuming a Λ CDM cosmology with $\Omega_{\text{M}}=0.27$, $\Omega_{\Lambda}=0.73$ and a Hubble constant of $H_0=75 \text{ km s}^{-1} \text{ Mpc}^{-1}$. Luminosity

distances were estimated using the cosmology calculator by Wright (2006). All errors are 1σ unless stated otherwise. Note that although in recent years slightly lower values of H_0 have been reported, in particular from the *Planck* measurements (Ade et al. 2014), we continue to use $H_0 = 75 \text{ km s}^{-1} \text{ Mpc}^{-1}$ in order to allow a direct comparison with luminosities of our other samples. The differences in luminosity between the two values are on the order of 20%.

2. Observations and data reduction

2.1. Sample Selection

BAL QSOs generally appear to be X-ray weak following the definitions by Brandt et al. (2000) and Gibson et al. (2009). Therefore, compared with other classes of AGN, X-ray observation of BAL QSOs appear to be rather sparse and only a small number of known BAL QSOs have been followed up in X-rays (e.g. Grupe et al. 2003; Saez et al. 2012). Usually this X-ray weakness is explained by strong intrinsic absorption in X-rays, typically of the order of several 10^{22} cm^{-2} (e.g. Grupe et al. 2003; Saez et al. 2012). However, some BAL QSO, like PG 1004+130 and PG 1700+518 may be intrinsically X-ray weak as pointed out by Luo et al. (2013). As recently reported by Luo et al. (2014), observations by NuStar revealed that intrinsic X-ray weakness seem to be quite common among BAL QSOs. The Luo et al. (2014) sample also contains several of BAL QSOs discussed in our paper: besides PG 1004+130 and PG 1700+518, as mentioned above, also IRAS 07598+6508, PG 0946+301, PG 1001+054, Mkn 231, and IRAS 14026+4341. In other words, these are BAL QSO analogies of PHL 1811 (e.g. Leighly et al. 2007). The best-suited X-ray observatory to at least detect a BAL QSO in X-rays is *Chandra* due its superior imaging qualities. On the other hand, the most efficient Optical/UV instrument in space is the UV-Optical telescope (UVOT, Roming et al. 2005) onboard *Swift* (Gehrels et al. 2004). The aim of this study is to combine these two missions to obtain spectral energy distributions for BAL QSOs which then can be compared with already existing X-ray and UV/Optical data from *Swift* observations of NLS1s. The *Swift* observations of most of the NLS1s have been already published

in Grupe et al. (2010). We cross-correlated the catalogue of *Chandra* observations of BAL QSOs performed as part of the Penn State ACIS-S Guaranteed Time Program with the *Swift* master observation catalogue. An additional requirement was that optical spectra were publicly available. Out of 306 sources that have *Chandra* PSU GTO time (PI G. Garmire) and *Swift* observations we found 11 BAL QSOs for which we also found existing optical spectroscopy data as listed in Table 1. The *Chandra* observations of the majority of these BAL QSOs were already published by Saez et al. (2012). The three sources not listed in Saez et al. (2012) are SDSS J073733+392037, PG1115+080, and SDSS J143748+432707.

2.2. *Chandra* Observations

The coordinates, redshift, luminosity distance, Galactic column density, reddening, and *Chandra* observing parameters of the 11 BAL QSOs are summarized in Table 1. The primary and secondary data were retrieved from the *Chandra* archive. All data analysis was done with CIAO version 4.6 using the most recent calibration data base 4.5.9. Source counts were extracted within a circle with a radius of $1.5''$ and background counts in a nearby source-free circular region with a radius of $15''$. We applied the CIAO tasks *mkrmf* and *mkarf* to create the appropriate redistribution matrix and ancillary response files, respectively. The X-ray spectra were analyzed using XSPEC version 12.7.1 (Arnaud 1996). For the majority of spectra we applied Cash statistics (Cash 1979) to perform the fits in XSPEC. Because the focus of this paper is on constructing the spectral energy distributions we only performed a simple spectral analysis of the X-ray data. A more detailed analysis of the *Chandra* spectra can be found in Saez et al. (2012). Here, we perform a homogeneous re-analysis of all the sources presented in this paper, including fits with intrinsic absorbers, such as a partial covering absorber.

2.3. *Swift* Observations

Table 2 presents the *Swift* observations including the start and end times and the total exposure times. The *Swift* X-ray telescope (XRT; Burrows et al. 2005) was operating in photon counting mode (Hill et al. 2004) and the data were reduced by the task *xrtpipeline* version

0.12.6., which is included in the HEASOFT package 6.12. Source counts were selected in a circle with a radius of $24.8''$ and background counts in a nearby circular region with a radius of $247.5''$. The X-ray spectra were analyzed using *XSPEC* version 12.7.1 (Arnaud 1996).

The UV-Optical Telescope (UVOT; Roming et al. 2005) data of each segment were coadded in each filter with the UVOT task *uvotimsum*. Source counts in all 6 UVOT filters were selected in a circle with a radius of $5''$ and background counts in a nearby source free region with a radius of $20''$. UVOT magnitudes and fluxes were measured with the task *uvotsource* based on the most recent UVOT calibration as described in Poole et al. (2008) and Breeveld et al. (2010). The UVOT data were corrected for Galactic reddening (Schlegel et al. 1998). The correction factor in each filter was calculated with equation (2) in Roming et al. (2009) who used the standard reddening correction curves by Cardelli et al. (1989).

Although *Swift* observations existed for most of these BAL QSOs, for 5 of these sources we requested new observations to obtain UVOT observations in all 6 UVOT filters. All these additional observations were performed in January and June 2014 and were typically of the order of 2ks as listed in Table 2.

2.4. Infrared data

In order to extend the spectral energy distributions to lower energies we obtained publicly available data in the near infrared from the Two Micron All-Sky Survey (2MASS, Skrutskie et al. 2006) and in the mid-infrared from the *Wide-field Infrared Survey Explorer* mission *WISE* (Wright et al. 2010). These infrared data were retrieved from the public archive at the Infrared Processing and Analysis Center using the online GATOR tool. The observed fluxes in the 2MASS J, H, K, and WISE W1, W2, W3, and W4 bands are listed in Table 3.

2.5. Optical Spectroscopic data

Optical spectra of the BAL QSOs were primarily derived from the Sloan Digital Sky Survey (SDSS York et al. 2000) Data Release 10 (DR10, Ahn et al. 2013), except for IRAS 07598+6508,

Mkn 231, PG 1700+518, and PG 2112+059. For these objects we used the optical spectra published in Hines & Wills (1995), Moustakas & Kennicutt (2006), and Boroson & Green (1992), respectively. For all measurements of optical line properties we subtracted an FeII template which was based on the Boroson & Green (1992) template, as described in Grupe et al. (2004a). For the black hole estimates we applied the relations given in Vestergaard & Peterson (2006) and Vestergaard & Osmer (2009).

3. Results

3.1. Analysis of the *Chandra* data

All *Chandra* data were fitted initially with an absorbed power law model with the Galactic absorption column density N_H listed in Table 1. While this model seems appropriate for most objects, 4 of the sources require an intrinsic absorber at the redshift of the source. While PG 0946+301 can be fitted by a simple neutral absorber, the other three BAL QSOs, PG 1004+130, PG1115+080, and Mkn 231 need be fitted by a partial covering absorber model. The results of all fits to the *Chandra* data are summarized in Table 4, including the X-ray fluxes in the 0.3-10 keV observed frame. In addition, Table 4 also lists the Optical to X-ray spectral slopes α_{ox} . These were determined based on the spectral energy distributions using the *Chandra* and *Swift* data as shown in Figure 1 (see Section 3.2). Note, however, that the spectral models used here are just a phenomenological description of the spectrum and do not necessarily represent the underlying physics in the source. For example, the geometry of Mkn 231 is highly complex consisting of absorption components as well as contributions from X-ray emission from strong surrounding starburst regions (e.g. Teng et al. 2014, and references therein). Nevertheless, our results obtained for PG 1004+130 agree well with those found from the combined *Chandra* and NuStar data in Luo et al. (2013).

3.2. Spectral Energy Distribution

The spectral energy distributions (SEDs) displayed in Figure 1 were constructed by using the WISE, 2MASS, *Swift* UVOT, and *Chandra* X-ray data. All SEDs are shown in rest-frame with

k-corrected luminosities¹. Note that for IRAS 14026+4341 the number of counts detected during the 1.5 ks *Chandra* observation was too low to obtain a spectral fit. We therefore only give one data point in the 0.3-10 keV regime in the SED which was determined from the count rate during the *Chandra* observation and converted to flux units assuming a standard AGN spectrum with $\alpha_X=1.0$ and Galactic absorption. The bolometric luminosities L_{bol} were measured by integrating over the k-corrected SEDs as shown in Figure 1 between $1\mu\text{m}$ and 10 keV ($10^{14} - 2 \times 10^{18}$ Hz). These bolometric luminosities are listed in Table 6. The SEDs were also used to determine α_{ox} . These Optical to X-ray spectral slopes are listed in Table 4 together with the expected value estimated from the k-corrected rest-frame luminosity density at 2500\AA applying equation (12) in Grupe et al. (2010). Four of the 11 BAL QSOs appear to be clearly X-ray weak following the definition by Brandt et al. (2000) with $\alpha_{\text{ox}} > 2.0$. The α_{ox} criterion for X-ray weakness, however, depends on luminosity. We also determined the difference between the measured α_{ox} and the expected value for the Optical-to-X-ray spectral slope $\alpha_{\text{ox,expected}}$ following the relation given in Grupe et al. (2010). As described in Gibson et al. (2009) this parameter is defined as $\Delta\alpha_{\text{ox}} = \alpha_{\text{ox}} - \alpha_{\text{ox,expected}}$ and for the BAL QSOs in our sample is listed in Table 4.

Although for BAL QSOs absorption is the first thought when a source is detected to be X-ray weak (e.g. Grupe et al. 2003), spectral analysis of the data for these four source does not suggest the presence of a strong absorber. Interestingly, the BAL QSOs in which an intrinsic absorber is clearly detected appear not to be X-ray weak. Alternatively, these sources could be heavily absorbed (i.e. Compton thick), and only a reflected fraction of the intrinsic emission is actually seen. Also, given the quality of the spectral data, a partial covering geometry cannot be excluded. In a partial covering absorber scenario only a fraction of the intrinsic continuum emission is seen directly, while the rest is strongly obscured. Also note again, that some of the BAL QSOs, like PG 1004+130 and PG 1700+518 may be intrinsically X-ray weak (Luo et al. 2013).

¹Applying the k-correction as defined by Oke & Sandage (1968) with $L_{\text{rest}} = L_{\text{obs}} \times (1+z)^{\alpha-1}$

3.3. Statistical Analysis

If BAL QSOs and NLS1s represent related phenomena, then some of their characteristic intrinsic properties should be similar. For our study we use the standard definition of NLS1s with a cut off line at $\text{FWHM}(\text{H}\beta)=2000 \text{ km s}^{-1}$.

3.3.1. Distributions

Figure 2 displays the box plots² of the distributions of observed and inferred properties of the whole sample (X-ray selected AGN sample of Grupe et al. (2010) plus the *Chandra*-selected BAL QSOs) on the bottom, NLS1s in the middle and BAL QSOs alone at the top. The mean, standard distribution, and median of these distributions are summarized in Table 7.

While the UV spectral indices of NLS1s and BAL QSOs are very similar, BAL QSOs show significantly flatter X-ray spectral slopes α_X , and steeper Optical to X-ray spectral slopes α_{ox} than NLS1s. There are several ways to interpret these properties. The flatter X-ray slopes in BAL QSOs may be a consequence of their slightly lower Eddington ratios than NLS1s, as suggested by the relations found by Grupe (2004); Grupe et al. (2010) and Shemmer et al. (2008). They may also imply stronger (cold or ionized) absorption, which was not yet detectable in available X-ray spectra due to short exposure times. The steeper α_{ox} can be primarily explained by stronger absorption in X-rays in BAL QSOs, for example by a partial covering absorber (e.g. Grupe et al. 2003). More importantly, BAL QSOs exhibit much larger $\Delta\alpha_{\text{ox}}$ parameters than NLS1s.

As for the emission line properties, we noticed that the $\text{FWHM}([\text{OIII}])$ of BAL QSOs are significantly larger than those of NLS1s. Note, that these broad NLR emission lines are consis-

² Box plots are a standard visualization tool in data mining to obtain information on the distribution of a parameter (e.g. Feigelson & Babu 2012; Torgo 2011; Crawley 2007). They allow a simple representation of the parameter distribution and how different samples compare. A boxplot consists of three parts: the box, the whiskers, and the outliers. The box displays the 1., 2. (median, solid line in the box), and 3. quartile of the distribution. The 'whiskers' are defined by the minimum/maximum values of the distribution or the 1.5 times the interquartile range (so the width of the box, so basically the 95% confidence level), whatever comes first. Values beyond the 'whiskers' are outliers and are displayed as circles.

tent with BAL QSOs being hosted in significantly larger galaxies. As we will see later, these [OIII] line widths are consistent with the black hole masses measured in BAL QSOs. The [OIII]/H β flux ratios in BAL QSOs are significantly lower than compared with NLS1s. The FeII/H β ratios of BAL QSOs are larger than those found in NLS1s. This follows the 'eigenvector 1' relation found by Boroson & Green (1992) in which AGN with stronger FeII emission show weaker emission from the NLR. Compared with the BAL QSO sample of Dietrich et al. (2009), the BAL QSOs in our sample here appear quite extreme in their [OIII]/H β and FeII/H β line ratios as listed in Table 7. The BAL QSOs in Dietrich et al. (2009) showed mean, standard deviations and medians of -0.63 , 0.29 , and -0.65 , and -0.12 , 0.42 , and -0.20 for \log [OIII]/H β and \log FeII/H β , respectively. These values are similar to those found for NLS1s (see Table 7). Note however, that the BAL QSOs in our sample for which optical line ratios could be determined are all at lower redshift, which the BAL QSOs in the Dietrich et al. (2009) sample are all at redshifts around $z=2$.

BAL QSOs have significantly larger black hole masses than NLS1s. In general, the black hole masses of BAL QSOs are about 100 times larger than those of NLS1s. What is somewhat surprising is that the Eddington ratios L/L_{Edd} of BAL QSOs are about a factor of 10 lower than we found in the NLS1s in our bright soft X-ray selected AGN sample. Figure 7 in Boroson (2002), however, suggested that the Eddington ratios of NLS1s and BAL QSOs are about unity.

Figure 7 in Boroson (2002) also suggests that the mass accretion rates \dot{M} of BAL QSOs and NLS1s are significantly different. As displayed in Figure 2 also when compare our BAL QSO and NLS1 samples we come to a similar conclusion. We estimated the mass accretion rate from the bolometric luminosity with $L_{\text{bol}} = \eta \dot{M} c^2$ assuming a mass to radiation efficiency of $\eta=0.1$. Also in our sample, BAL QSOs have larger mass accretion rates than NLS1s. Note that some of these mass accretion rates in BAL QSOs exceed $100 M_{\odot}/\text{year}$.

3.3.2. Correlations

Figure 3 displays the relation between the Eddington ratio L/L_{Edd} and the mass accretion rate \dot{M} following Figure 7 in Boroson (2002). In

Figure 3 the BAL QSOs of the Chandra sample are displayed as magenta stars, NLS1s as solid blue triangles, BLS1s as solid red circles, and the BAL QSOs of Dietrich et al. (2009) are shown as turquoise crosses. Clearly, BAL QSOs and NLS1s fall on two separated groups. For a given L/L_{Edd} , BAL QSOs have a significantly larger mass accretion rate than NLS1s. This is not completely surprising given the fact that the black hole masses of NLS1s is about a factor of 100 lower than that of BAL QSOs (see also the distributions of black hole masses in Figure 2). However, the plot also shows that the schematic plot shown in Figure 7 in Boroson (2002) is too simple. Although generally speaking, BAL QSOs have higher mass accretion rates than NLS1s, as already shown in Figure 2, there is some overlap between the two groups and the separation between the two classes of AGN is not as strong as suggested in Figure 7 in Boroson (2002). The other difference is that the BAL QSOs in our sample appear to have lower L/L_{Edd} than in the Boroson (2002) sample. The lower L/L_{Edd} found in our BAL QSO sample is similar to those found in the BAL QSOs in Dietrich et al. (2009).

3.3.3. Principal Component Analysis

In order to better understand the relations among the observed parameters we applied a Principal Component Analysis (PCA; Pearson 1901). to the sample of 119 AGN, including the Swift AGN sample plus the 7 low-redshift BAL QSOs listed in Table 1. A PCA is a standard data mining tool that allows to reduce the number of properties that describe a sample of sources from many to a few. In a mathematical sense, the PCA searches for the eigenvalues and eigenvectors in a correlation coefficient matrix. A good description for the application of a PCA in astronomy can be found in Wills & Francis (1999) and Boroson & Green (1992).

For our sample we used α_{X} , α_{UV} , α_{ox} , $\Delta\alpha_{\text{ox}}$, $\text{FWHM}(\text{H}\beta)$, $\text{FWHM}([\text{OIII}])$, $[\text{OIII}]/\text{H}\beta$, $\text{FeII}/\text{H}\beta$ as input parameters in the PCA. The results of the PCA are summarized in Table 8. This PCA is somewhat similar to the one that we applied to basically the same AGN sample in Grupe (2004), although with slightly different input parameters.

Figure 5 displays the correlations between eigenvector 1 and L/L_{Edd} , and eigenvector 2 and the black hole mass and \dot{M} . While the eigenvector

1 of our sample can be associated with the Eddington ratio L/L_{Edd} (left panel), such as in the PCA performed by Boroson (2002), the eigenvector 2 of our sample is clearly dominated by the black hole mass (middle panel). The Spearman rank order correlation coefficients, Student's T-test values, and probabilities of a random result of the eigenvector 1 - L/L_{Edd} and eigenvector 2 - M_{BH} correlations are $r_s = -0.52$, $T_s = -6.62$, $P < 10^{-8}$, and $r_s = -0.82$, $T_s = -15.04$, $P < 10^{-8}$, respectively.

Although the mass accretion rate is anti-correlated with eigenvector 2 (right panel) with $r_s = -0.32$, $T_s = -3.64$, $P = 4.1 \times 10^{-4}$, it is in our sample also anti-correlated with eigenvector 1 ($r_s = -0.44$, $T_s = -5.32$, $P = 5.2 \times 10^{-7}$). However, eigenvectors are orthogonal, which means they should not show a correlation among them. Therefore we conclude that in our sample eigenvector 2 represents the black hole mass and not \dot{M} . Note, that for his input sources and input parameters, Boroson (2002) concluded from his PCA that eigenvector 2 represents the mass accretion rate \dot{M} . As a test we performed a PCA with just the optical line properties (FWHM($\text{H}\beta$), FWHM([OIII]), [OIII]/ $\text{H}\beta$, and FeII/ $\text{H}\beta$). In this case the correlation between eigenvector 2 and \dot{M} becomes more significant with $r_s = -0.46$, $T_s = -5.67$, $P = 1.0 \times 10^{-7}$. However, the correlation between eigenvector 2 and the black hole mass is still stronger than that with \dot{M} .

4. Discussion

The main motivation behind this study is the question of whether BAL QSOs and NLS1s are intrinsically similar but only appear at different ends of the black hole mass distribution spectrum as suggested by Brandt & Gallagher (2000) and Boroson (2002). Although we see similarities between our sample and that of Boroson (2002), in particular that NLS1s and BLA QSOs have similar FeII/ $\text{H}\beta$ and [OIII]/ $\text{H}\beta$ line ratios we also notice differences in the studies.

4.1. Selection Effects

While our sample size is significantly larger than the initial exploratory study of Boroson (2002), it is still subject to selection effects, and we therefore first address the key question, if and how our sample selection affects the parameters we

wish to compare among NLS1s and BAL-QSOs:

1. **Redshift Distributions:** Traditionally, BAL QSOs have been discovered at redshifts of about $z=2$ (e.g. Weymann et al. 1991). This leads to selecting highly-luminous and therefore high black hole mass AGN. On the other hand, our AGN sample consists of bright X-ray selected AGN which appear at much lower redshifts with $z < 0.4$ (Grupe et al. 2004a; Grupe et al. 2010). Nevertheless, the 7 low redshift BAL QSOs presented in this paper have redshifts that are between $z=0.04$ and $z=0.47$ and fall into the redshift range of our AGN sample. This redshift range is also comparable to the PG sample by Boroson & Green (1992) which contains the BAL QSOs used in Boroson (2002) sample. The 7 low-redshift BAL QSOs in our sample allow a direct comparison to the low-redshift AGN sample by Grupe et al. (2004a) and Grupe et al. (2010) which is not necessarily true for the high-redshift objects.
2. **Soft X-ray selection of the AGN sample:** Our AGN sample was selected by their X-ray properties: X-ray bright and soft X-ray spectra (Grupe et al. 1998; Grupe et al. 2001; Grupe et al. 2004a; Grupe et al. 2010). A steep X-ray spectrum, however, is a consequence of high Eddington ratios (Grupe 2004; Grupe et al. 2010; Shemmer et al. 2008). Therefore the soft X-ray selection favors sources with high L/L_{Edd} among the class of NLS1 galaxies as a whole and the Eddington ratios found in our AGN sample may appear larger than in an optically selected NLS1 sample. The soft X-ray selection also misses highly absorbed AGN, such as typically BAL QSOs.

Although we have to keep these selection effects in mind, they do not make our study invalid. On the contrary, our comparison is between BAL QSOs and NLS1s, and the latter are usually found among soft X-ray selected AGN. It has also been shown that in BAL QSOs and in NLS1s absorbers can develop over time and the absorption column density and covering fraction can vary in X-rays as well as in the UV. For NLS1s a good

example here is WPVS 007 which has developed strong BALs within a decade (Leighly et al. 2009). On the other hand, more and more evidence has been found that also the BALs in BAL QSOs can be highly variable (Filiz Ak et al. 2012, 2013; Capellupo et al. 2011, 2012, e.g.).

4.2. Mass accretion rate \dot{M}

While Figure 7 in Boroson (2002) suggests that NLS1s and BAL QSOs are both at high L/L_{Edd} where BAL QSOs have significantly larger mass accretion rates than NLS1s, we found from our sample that this picture is more complicated: Although also in our sample BAL QSOs appear to show the highest mass accretion rates, some appear to be significantly lower, even down to $0.1 M_{\odot}/\text{year}$ in the case of PG 1004+130. Compared with the BAL QSOs in Dietrich et al. (2009), where the mean mass accretion rate was of the order of about $35 M_{\odot}/\text{year}$, the mass accretion rates in the sample presented here appear to be rather modest with a median of about $4 M_{\odot}/\text{year}$. However, some of the mass accretion rates of the BAL QSOs in our sample are extreme, exceeding $100 M_{\odot}/\text{year}$. The distribution of the mass accretion rates in BAL QSOs spans over three orders of magnitude as shown in Figure 2. Although the mass accretion rate of NLS1s also stretches over three orders of magnitude, the lowest values of the mass accretion rate are of the order of 10^{-3} solar masses and the highest of the order of a few solar masses per year. There is a some overlap between NLS1s and BAL QSOs in mass accretion rate in our sample. The two samples are not as separated as the BAL QSO and NLS1s samples of Boroson (2002). This maybe in part a selection effect, because the NLS1s in our sample are soft X-ray selected which are primarily sources with high L/L_{Edd} .

If we just focus on the 7 low-redshift BAL QSOs in our study (see Table 1) we notice that the mass accretion rates of these BAL QSOs are in the range between 0.1 to $8 M_{\odot}/\text{year}$ and are somewhat comparable to the mass accretion rates seen in NLS1s. The BAL QSOs which really make a difference are those at higher redshifts.

We noticed that the mass accretion rates in BAL QSOs is rather high with more than $100 M_{\text{sun}} \text{ yr}^{-1}$, and 35 in the BAL QSO sample by Dietrich et al. (2009). One reason why these accretion rates appear so high might be our assumption

of the mass to radiation efficiency which we for simplicity just set to $\eta = 0.1$. If however the black hole spin in BAL QSOs is significantly higher this would increase the efficiency and reduce the mass accretion rate necessary to explain the observed bolometric luminosity. For example, if the black hole in a BAL QSO is maximal spinning ($a=0.998$) the efficiency will be $\eta = 0.32$, or three times higher than our assumed $\eta=0.1$. This would imply that the mass accretion rate is a factor of 3 lower, which is much easier to explain than the high mass accretion rates we estimated at first. In contrast to BAL QSOs, in NLS1s the efficiency may be lower and the mass accretion rate higher if the black hole is rotating slower than in our assumption. Keep in mind that for an efficiency of $\eta = 0.1$ the black hole is spinning already with $a=0.6$. One argument that the black hole spins in BAL QSOs and NLS1s are systematically different, is the finding that the black hole masses in BAL QSOs are significantly larger than in NLS1s. A larger black hole mass also means that the accreted matter has transferred a larger amount of angular momentum to this black hole which then results in a larger spin (in a scenario where SMBHs primarily grow by accretion). One more argument for a higher efficiency of the mass to radiation conversion due to a relativistically spinning black hole is that the mass accretion rates in the sample presented here appear to be relatively low compared with those of the BAL QSO sample by Dietrich et al. (2009).

4.3. Eddington ratios L/L_{Edd}

The BAL QSOs in our sample also have Eddington ratios L/L_{Edd} which are lower than those of NLS1s. In Figure 7 in Boroson (2002) shows that the BAL QSOs in the Boroson & Green (1992) sample are all at $L/L_{\text{Edd}}=1$, which is typical for NLS1s. Although our AGN/NLS1 sample is soft X-ray selected and has therefore a bias towards high L/L_{Edd} AGN, the Eddington ratios found in our sample agree well with those of the NLS1s in the optically selected sample by Boroson & Green (1992). However, a comparison between our sample and that of Boroson (2002) appears somewhat difficult because Boroson & Green (1992) do not list the values of L/L_{Edd} and \dot{M} of the NLS1s and BAL QSOs of their PG quasar sample.

Although the eigenvector 1 in our PCA can also

be associated with the Eddington ratio L/L_{Edd} as in the Boroson (2002) sample, our eigenvector 2 seems to be different. While Boroson (2002) suggested that the eigenvector 2 in his sample is clearly associated with the mass accretion rate \dot{M} , in our sample eigenvector 2 is more strongly correlated with the black hole mass. These differences are not surprising. A PCA is a purely mathematical tool and the results depend strongly on the set of input parameters as well as the objects in the sample. While in our PCA we used continuum properties and line widths and ratios, the PCA in Boroson (2002) primarily used optical line properties. Therefore it can be expected that the results of the PCAs could be different. However, when we only use optical line parameters in a PCA, we still find that in our sample that eigenvector 2 is strongly correlated with the black hole mass.

4.4. Black Hole Masses and Growth

From our BAL QSO and NLS1 samples we found that BAL QSOs have black hole masses more than 100 times larger than those seen in a typical NLS1. At first glance this seems to be a selection effect because most BAL QSOs appear at higher redshifts which leads to selecting objects with higher luminosities and larger black hole masses. However, for low-redshift BAL QSOs in our *Chandra* sample, we note that even these objects have black hole masses of the order of $10^9 M_{\odot}$, significantly larger than those found in NLS1s (see Figure 2).

In contrast to NLS1s, BAL QSOs may have already fully developed black holes with regards to their host galaxy masses. This argument is supported by the $M - \sigma$ relation which relates the mass of the central black hole to that of the host galaxy. BAL QSOs fall right on the Tremaine et al. (2002) $M - \sigma$ relation as shown in in Figure 6 (the Tremaine et al. (2002) relation is shown as a black solid line), while NLS1s typically fall below this relation (Grupe & Mathur 2004). We adopted the method introduced by Nelson (2000) who suggested to use the [OIII] line as a proxy of the stellar velocity dispersion in the host galaxy bulge³. Because the Narrow

Line Region is in the gravitational potential of the host galaxy bulge, the NLR gas follows the same velocity dispersion as the bulge stars. As a comparison we also show the BAL QSOs from the study by Dietrich et al. (2009) in this plot. Note that the BAL QSO of the Dietrich et al. (2009) sample have redshifts between $z=1-2$ and from our BAL QSO sample we have only [OIII] and $H\beta$ measurements of the 7 low-redshift BAL QSOs. The BAL QSOs of our sample which are at higher redshifts also have similar black hole masses as the objects in the Dietrich et al. (2009) BAL QSO sample. Whether NLS1 galaxies, as a group, fall on or below the $M - \sigma_{[\text{OIII}]}$ relation is an important question (e.g. Grupe & Mathur 2004; Mathur & Grupe 2005a,b; Komossa & Xu 2007). The only BAL QSO that falls below the $M - \sigma_{[\text{OIII}]}$ relation is PG 1001+054. The (soft X-ray selected) NLS1 sample of Grupe & Mathur (2004) was located significantly below the $M - \sigma_{[\text{OIII}]}$ relation, while the NLS1 sample of Komossa & Xu (2007) was consistent with the $M - \sigma_{[\text{OIII}]}$ relation of non-active galaxies, with the exception of sources at high L/L_{Edd} . These had their whole [OIII] emission systematically blueshifted (“blue outliers”), implying large outflows which come with a strong extra line broadening apparently displacing them from the $M - \sigma_{[\text{OIII}]}$ relation. Therefore the FWHM([OIII]) measured in these objects may not represent the velocity of the velocity dispersion in the bulge, but has an additional, unknown contribution by outflows. In the same way as turbulent motion can lead to an overestimation of the the black hole masses from BLR emission line widths as shown by Kollatschny & Zetzl (2011), an outflow adds an additional velocity component to the total velocity and therefore leads to an overestimation of the mass of the host galaxy bulge.

4.5. Outflows in BAL QSOs and NLS1s

The main question remaining is why do we see strong outflows which appear as deep UV absorption troughs in BAL QSOs but these are rarely seen in NLS1s. In a matter of fact, the only NLS1s that has shown dramatic UV absorption troughs is WPVS 007. Part of the answer maybe that BAL QSOs are highly-luminous AGN and as shown by Laor & Brandt (2002), the strengths of the BAL troughs correlates with luminosity. Nev-

³We assign the expression $\sigma_{[\text{OIII}]}$ for the stellar velocity dispersion determined from the width of the [OIII] $\lambda 5007\text{\AA}$ line.

ertheless, the NLS1 WPVS 007 is a low luminosity AGN and seems to contradict these findings. Strong outflows are typically associated with high L/L_{Edd} which results in a strong radiation field from the accretion disk producing radiation driven winds/outflows Proga & Kallman (e.g. 2004); Kurasawa & Proga (e.g. 2009a,b). On the other hand, NLS1s with high L/L_{Edd} exhibit strong outflows through their broad, blueshifted [OIII] emission lines (e.g. Bian et al. 2005; Zhang et al. 2011; Xu et al. 2012), which we do not see in BAL QSOs (e.g. Dietrich et al. 2009).

4.6. Overall Comparison and Conclusions

One reason for the slight differences between our study and that by Boroson (2002) maybe the different sample sizes. While in our sample we have 11 BAL QSOs (7 at low redshift) and 53 NLS1s, the numbers in the Boroson (2002) sample are 4 BAL QSOs and 8 NLS1s. The low number of in particular BAL QSOs may have a large influence on these differences. As mentioned about, the mass accretion rates in other BAL QSO samples, like that in Dietrich et al. (2009) appear to be larger. Therefore in a sample of just 4 sources, the chance of selecting BAL QSOs with larger mass accretion rates is quite high.

To conclude, we confirm the results by Brandt & Gallagher (2000) and Boroson (2002) about the differences in the black hole mass distributions between BAL QSOs and NLS1s. We also confirm that the Eddington ratios of BAL QSOs and NLS1s are at the higher end of the L/L_{Edd} distribution of AGN in general. However, from our samples of NLS1s and BAL QSOs the Eddington ratios NLS1s typically operate around unity, while those of the BAL QSOs are slightly lower. NLS1s and BAL QSO also share that their $\text{FeII}/\text{H}\beta$ ratios are very high and their $[\text{OIII}]/\text{H}\beta$ ratios are low - following the 'classic Boroson & Green (1992)' eigenvector 1 relation. Although some BAL QSOs in our sample exhibit very high mass accretion rates inferred from their bolometric luminosities, the mass accretion rates of BAL QSOs and NLS1s appear to be more similar than previously thought. This is in particular true when we look at the low redshift BAL QSOs in our sample. Interestingly, even though BAL QSOs have relatively large L/L_{Edd} ratios, they fall right onto the $M_{\text{BH}} - \sigma_{[\text{OIII}]}$ relation suggesting that they have fully developed

black holes. One reason for the large bolometric luminosities found in BAL QSOs may be that the black hole is spinning relativistically which leads to a significantly higher efficiency of the mass to radiation conversion. In the future we need to increase the number of BAL QSOs in our study to obtain better statistics on the relations found in our study. In particular we need to obtain more X-ray observations of BAL QSOs to measure the continuum properties. And last but not least, in the far future we need to study the Fe K α line emission line to study the gravitational and relativistic effects which can be used to measure the black hole spin.

We would like to thank Neil Gehrels for approving our ToO requests and the *Swift* team for performing the ToO observations. We thank our anonymous referee for useful comments and suggestions which have improved the paper significantly. In particular we want to thank S. Komossa for very valuable discussions and comments on this paper. Many thanks to Bev Wills for providing the optical spectrum of IRAS 07598+6508 (Hines & Wills 1995). We also thank Matthias Dietrich for providing the optical line fluxes for the BAL QSOs reported in Dietrich et al. (2009), and Leisa Townsley for supporting this project. This research has made use of the NASA/IPAC Extragalactic Database (NED) which is operated by JPL, Caltech, under contract with NASA. This publication makes use of data products from the Wide-field Infrared Survey Explorer, which is a joint project of the University of California, Los Angeles, and JPL, funded by NASA. This publication makes use of data products from the Two Micron All Sky Survey, which is a joint project of the University of Massachusetts and the Infrared Processing and Analysis Center/California Institute of Technology, funded by NASA and NSF. The scientific results reported in this article are based partly on data obtained from the Chandra Data Archive. This research has made use of software provided by the Chandra X-ray Center (CXC) in the application package CIAO. This research has made use of the XRT Data Analysis Software (XRTDAS) developed under the responsibility of the ASI Science Data Center (ASDC), Italy. *Swift* at PSU is supported by NASA contract NAS5-00136 (DG + JN). This work was sup-

ported by the Penn State ACIS Instrument Team Contract SV4-74018, issued by the Chandra X-ray Center, which is operated by the Smithsonian Astrophysical Observatory for and on behalf of NASA under contract NAS8-03060. The Guaranteed Time Observations (GTO) included here were selected by the ACIS Instrument Principal Investigator, Gordon P. Garmire, of the Huntingdon Institute for X-ray Astronomy, LLC, which is under contract to the Smithsonian Astrophysical Observatory; Contract SV2-82024.

REFERENCES

- Ade, P.A.R., et al., 2014, A&A, in press, arXiv:1303.5076v3
- Ahn, C.P., et al., ApJS, submitted, arXiv:1307.7735
- Arnaud, K. A., 1996, ASP Conf. Ser. 101: Astronomical Data Analysis Software and Systems V, 101, 17
- Becker, R.H., et al., 2000, ApJ, 538, 72
- Bian, W.; Yuan, Q.; Zhao, Y., 2005, MNRAS, 364, 187
- Boroson, T.A., & Green, R.F., 1992, ApJS, 80, 109
- Boroson, T.A., & Meyers, K.A., 1992, ApJ, 397, 442
- Boroson, T.A., 2002, ApJ, 565, 78
- Brandt, W.N., Laor, A., & Wills, B.J., 2000, ApJ, 528, 637
- Brandt, W.N., & Gallagher, S.C., 2000, New Astronomy Review 44, 461
- Breeveld, A.A., et al., 2010, MNRAS, 406, 1687
- Burrows, D., et al., 2005, Space Science Reviews, 120, 165
- Capellupo, D.M., et al., 2011, MNRAS, 413, 908
- Capellupo, D.M., Hamann, F., Shields, J.C., Rodriguez Hildago, P., & Barlow, T.A., 2012, MNRAS, 422, 3249
- Cardelli, J.A., Clayton, G.C., Mathis, J.S., 1989, ApJ, 345, 245
- Cash, W., 1979, ApJ, 228, 939
- Crawley, M.J., 2007, The R Book, Wiley & Sons
- Crenshaw, D., Kraemer, S., & Gabel, J., 2004, ASPC, 311, 235
- Cooper, E.M., Leighly, K.M., Hamann, F., & Grupe, D., 2013, Proc. "Nuclei of Seyfert Galaxies and QSOs - Central engine and conditions of star formation", Bonn, November 2012, Proceedings of Science, in press
- Dai, X., Shankar, F., & Sivakoff, G.R., 2008, ApJ, 672, 108
- Dietrich, M., et al., 2009, ApJ, 696, 1998
- Elvis, M., 2000, ApJ, 545, 63
- Feigelson, E.D., & Babu, G.j., 2012, "Modern Statistical Methods for Astronomy", Cambridge University Press
- Filiz Ak., N., et al., 2012, ApJ, 757, 114
- Filiz Ak., N., et al., 2013, ApJ, 777, 168
- Gallo, L.C., et al. 2013, MNRAS, 438, 1191
- Gehrels, N., et al., 2004, ApJ, 611, 1005
- Giannuzzo, M.E., & Stirpe, G.M., 1996, A&A, 314, 419
- Gibson, R.R., et a., 2009, ApJ, 692, 758
- Goodrich, R.W., 1989, ApJ, 342, 224
- Goodrich, R.W., 2000, New Astronomy reviews, Vol 44, 519
- Grupe, D., 2004, AJ, 127, 1799
- Grupe, D., Beuermann, K., Mannheim, K., Thomas, H.-C., de Martino, D., & Fink, H.H., 1995, A&A, 300, L21
- Grupe, D., Beuermann, K., Thomas, H.-C., Mannheim, K., & Fink, H.H., 1998, A&A 330, 25
- Grupe, D., Beuermann, K., Mannheim, K., & Thomas, H.-C., 1999, A&A, 350, 805
- Grupe, D., Thomas, H.-C., & Beuermann, K., 2001, A&A, 367, 470

- Grupe, D., & H.-C. Thomas, 2002, *A&A*, 386, 854
- Grupe, D., Mathur, S., & Elvis, M., 2003, *AJ*, 126, 1159
- Grupe, D., & Mathur, S., 2004, *ApJ*, 606, L41
- Grupe, D., Wills, B.J., Leighly, K.M., & Meusinger, H., 2004a, *AJ*, 127, 156
- Grupe, D., Schady, P., Leighly, K.M., Komossa, S., O’Brien, P.T., & Nousek, J.A., 2007a, *AJ*, 133, 1988
- Grupe, D., Komossa, S., & Gallo, L.C., 2007b, *ApJ*, 668, L111
- Grupe, D., Komossa, S., Gallo, L.C., Fabian, A.C., Larsson, J., Pradhan, A.K., Xu, D., & Miniutti, G., 2008, *ApJ*, 681, 982
- Grupe, D., Leighly, K.M., & Komossa, S., 2008, *AJ*, 136, 2343
- Grupe, D., Komossa, S., Leighly, K.M., & Page, K.L., 2010, *ApJS*, 187, 64
- Grupe, D., Komossa, S., Gallo, L.C., Longinotti, A.L., Fabian, A.C., Pradhan, A.K., Gruberbauer, M., & Xu, D., 2012, *ApJS*, 199, 28
- Grupe, D., Komossa, S., Scharwächter, J., Dietrich, M., Leighly, K.M., Lucy, A., & Barlow, B., 2013, *AJ*, 146, 78
- Hamann, F., Kaplan, K.F., Rodriguez Hildago, P., Prochaska, J.X., & Herbert-Fort, S., 2008, *MNRAS*, 391, L39
- Hill, J.E., et al., 2004, *SPIE*, 5165, 217
- Hines, D.C., & Wills, B.J., 1995, *ApJ*, 448, L69
- Kalberla, P.M.W., et al., *A&A*, 440, 775
- Kaspi, S., Smith, P. S., Netzer, H., Maoz, D., Januzzi, B. T., & Givon, U., 2000, *ApJ*, 533, 631
- Kollatschny, W., & Zetzl, M., 2011, *Nature*, 470, 366
- Komossa, S., & Xu, D., 2007, *ApJ*, 667, L33
- Komossa, S., 2008, *RMxAC*, 32, 86
- Komossa, S., et al., 2008a, *ApJ*, 678, L13
- Kraft, R.P., Burrows, D.N., & Nousek, J.A., 1991, *ApJ*, 374, 344
- Kurasawa, R., & Proga, D., 2009a, *ApJ*, 693, 1929
- Kurasawa, R., & Proga, D., 2009b, *MNRAS*, 397, 1791
- Laor, A., & Brandt, W.N., 2002, *ApJ*, 569, 641
- Leighly, K.M., Halpern, J.P., Jenkins, E.B., Grupe, D., Choi, J., & Prescott, K.B., 2007, *ApJ*, 663, 103
- Leighly, K.M., Hamann, F., Casebeer, D.A., & Grupe, D., 2009, *ApJ*, 701, 176
- Longinotti, A.L., et al., 2013, *ApJ*, 766, 104
- Luo, B., et al., 2013, *ApJ*, 772, 153
- Luo, B., et al., 2014, *ApJ*, accepted, arXiv:1408.3633v1
- Marziani, P., et al., 2009, *A&A*, 495, 83
- Mathur, S., 2000, *MNRAS*, 314, L17
- Mathur, S., & Grupe, D., 2005a, *A&A*, 432, 463
- Mathur, S., & Grupe, D., 2005b, *ApJ*, 633, 688
- Moustakas, J., & Kennicutt, R.C., 2006, *ApJS*, 164, 81
- Nelson, C.H., 2000, *ApJ*, 544, L91
- Oke, J.B., & Sandage, A., 1968, *ApJ*, 154, 21
- Osterbrock, D.E., & Pogge, R.W., 1985, *ApJ*, 297, 166
- Pearson, K., 1901, *Philosophical Magazine* 2 (6), 559
- Peterson, B.M., 1997, “Active Galactic Nuclei”, Cambridge University Press
- Poole, T.S., et al., 2008, *MNRAS*, 383, 627
- Proga, D., & Kallman, T.R., 2004, *ApJ*, 616, 688
- Roming, P.W.A., et al., 2005, *Space Science Reviews*, 120, 95
- Roming, P.W.A., et al., 2009, *ApJ*, 690, 163
- Saez, C., Brandt, W.N., Gallagher, S.C., Bauer, F.E., & Garmire, G.P., 2012, *ApJ*, 759, 42

- Schlegel, D. J., Finkbeiner, D. P., & Davis, M. 1998, *ApJ*, 500, 525
- Shemmer, O., Brandt, W.N., Netzer, H., Maiolino, R., & Kaspi, S., 2008, *ApJ*, 682, 81
- Skrutskie, M.F., et al., 2006, *AJ*, 131, 1163
- Sulentic, J.W., Zwitter, T., Marziani, P., & Dultzin-Hacyan, D., 2000, *ApJ*, 536, L5
- Tananbaum, H., et al., 1979, *ApJ*, 234, L9
- Teng, S.H., et al., 2014, *ApJ*, 785, 19
- Torgo, L., 2011, “Data Mining in R”, Chapman & Hall/CRC
- Tremaine, S., et al., 2002, *ApJ*, 574, 740
- Vestergaard, M., & Peterson, B.M., 2006, *ApJ*, 641, 689
- Vestergaard, M., & Osmer, P.S., 2009 *ApJ*, 699, 800
- Voges, W., Aschenbach, B., Boller, T., et al., 1999, *A&A*, 349, 389
- Weymann, R.J., Morris, L., Foltz, C.B., & Hewitt, P.C., 1991, *ApJ*, 373, 23
- Wills, B.J., & Francis, P.J., 1999, ASP Conference Series 162, Edited by Gary Ferland and Jack Baldwin, 363
- Wright, E.L., 2006, *PASP*, 118, 1711
- Wright, E.L., et al., 2010, *AJ*, 140, 1868
- Xu, D., et al., 2012, *AJ*, 143, 83
- York, D.G., et al., 2000, *AJ*, 1579
- Zamfir, S., Sulentic, J.W., Marziani, P., & Dultzin, D., 2010, *MNRAS*, 403, 1759
- Zhang, K., Dong, X.-B., Wang, T.-G., & Gaskell, C.M., 2011, *ApJ*, 737, 71

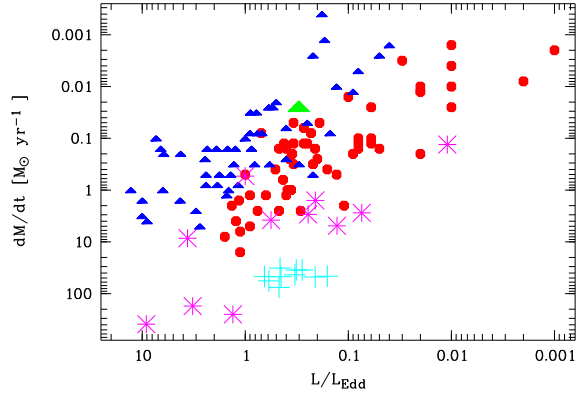


Fig. 3.— Eddington ratio L/L_{Edd} vs. mass accretion rate \dot{M} . BAL QSOs are displayed as large magenta stars, NLS1s as blue solid triangles and BLS1s as red solid circles. WPVS 007 is marked as a large solid green triangle. The cyan crosses mark the BAL QSOs from the sample of Dietrich et al. (2009) as a comparison.

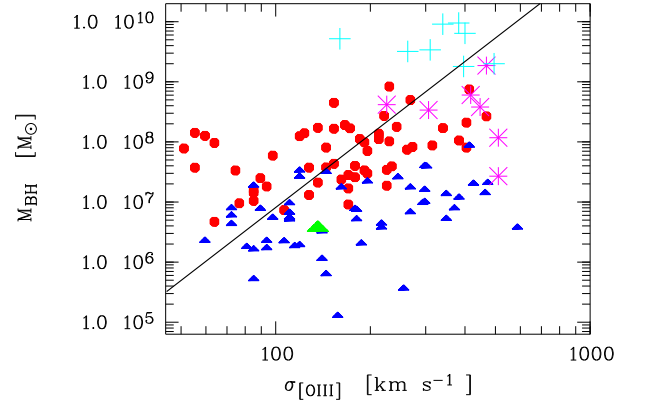


Fig. 6.— $M - \sigma$ relation for the AGN and BAL QSOs in the sample. The symbols are the same as defined in Figure 3. The cyan crosses mark the BAL QSOs from the sample of Dietrich et al. (2009) as a comparison.

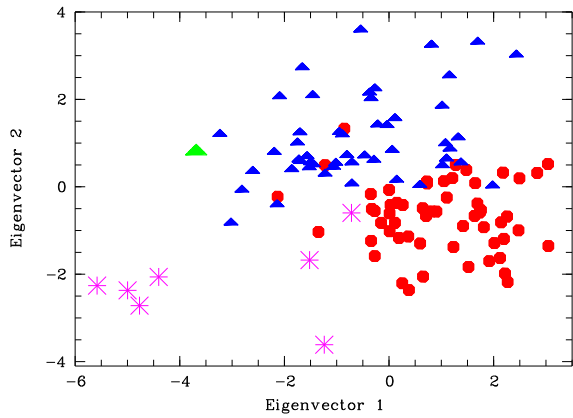


Fig. 4.— Eigenvector 1 vs. Eigenvector 2 diagram. The symbols are the same as defined in Figure 3.

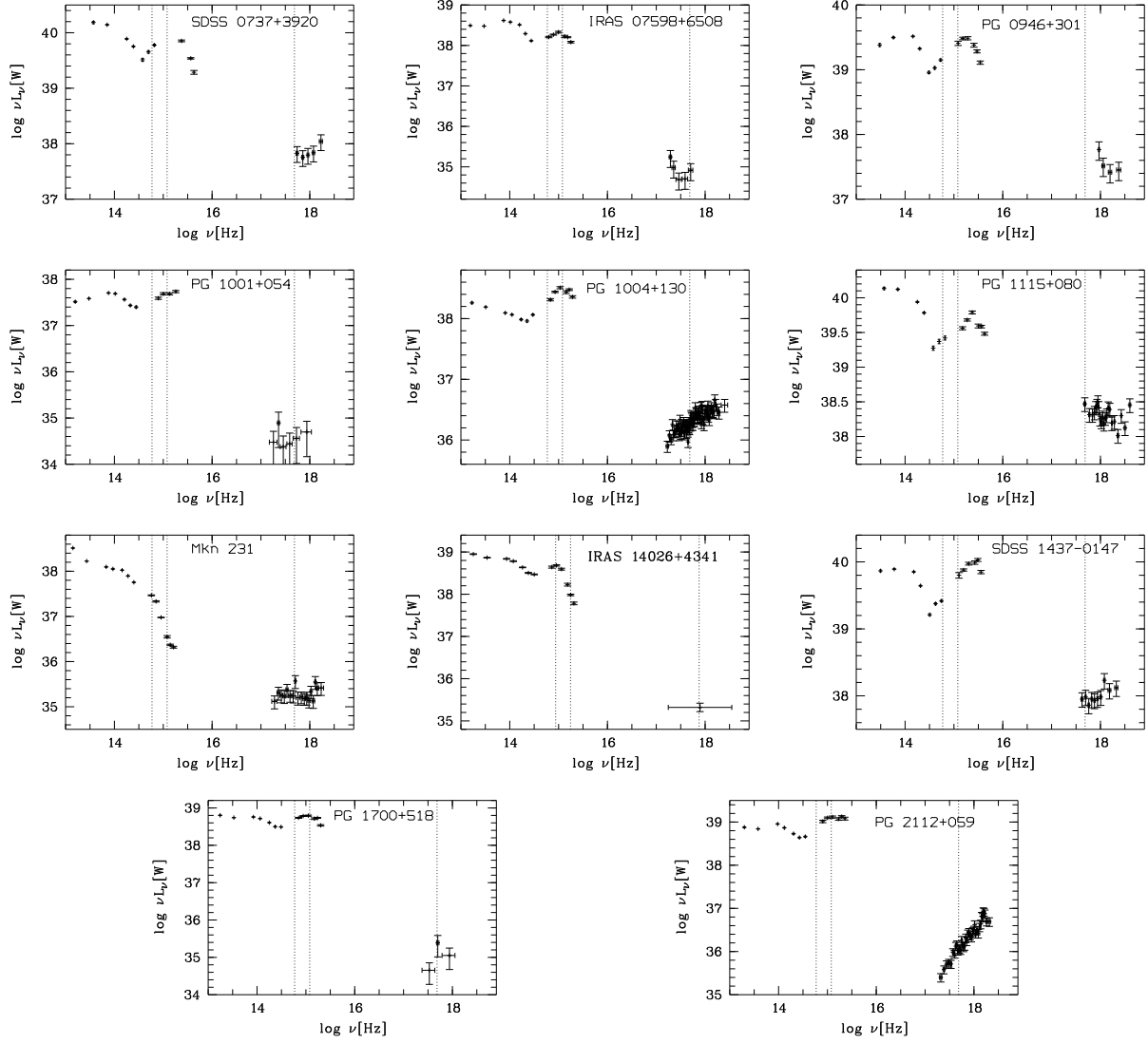


Fig. 1.— Rest-frame k-corrected IR to X-ray Spectral Energy Distributions of the BAL QSOs. The vertical dashed lines make the rest-frame 5500Å, 2500Å, and 2keV points. *Swift* UVOT and XRT data have been corrected for Galactic reddening and absorption.

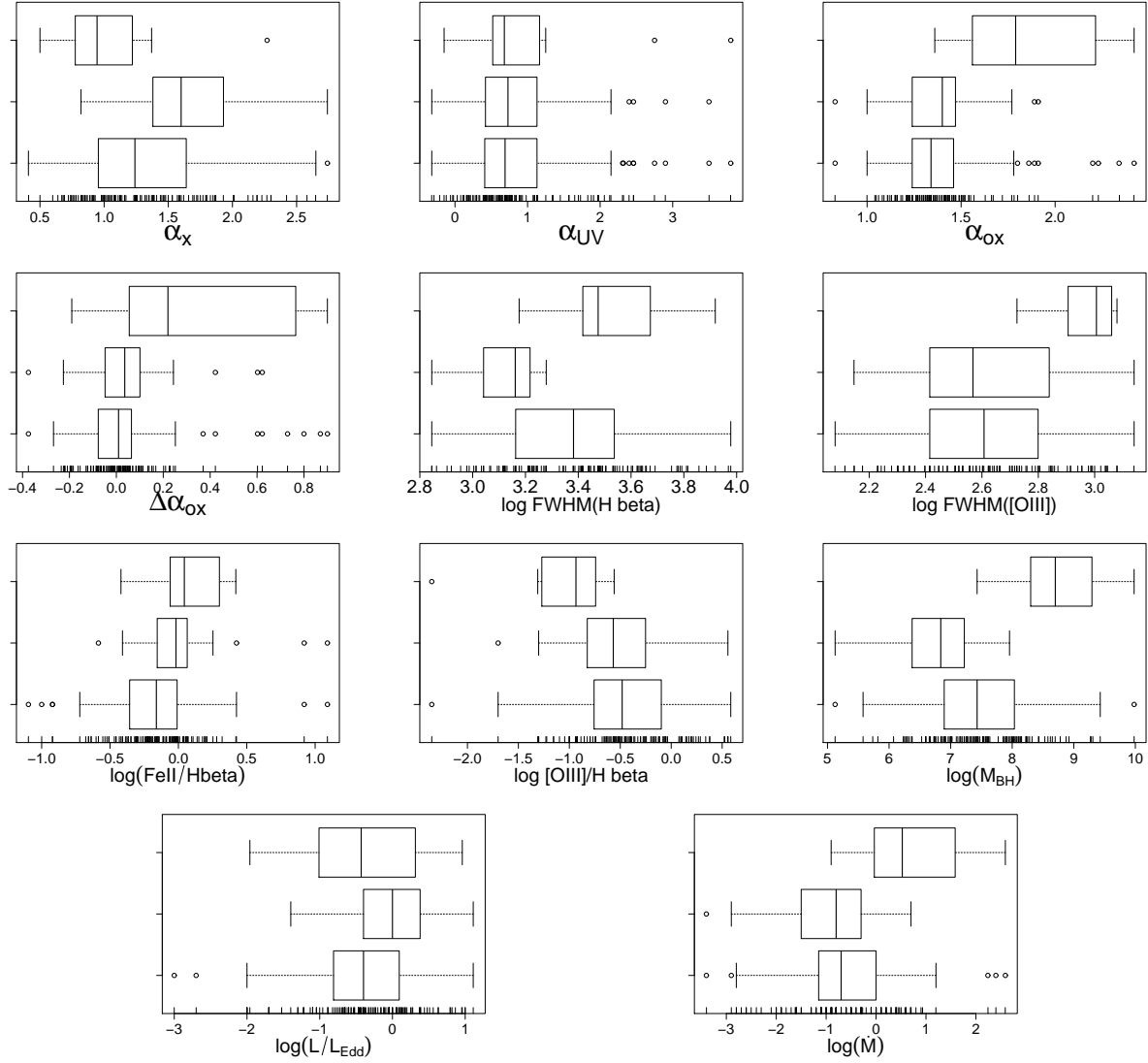


Fig. 2.— Box plots of the distributions of the whole AGN (X-ray selected sample by Grupe et al. (2010) and BAL QSOs) at the bottom, 'classical' NLS1s in the middle, and BAL QSOs alone at the top.

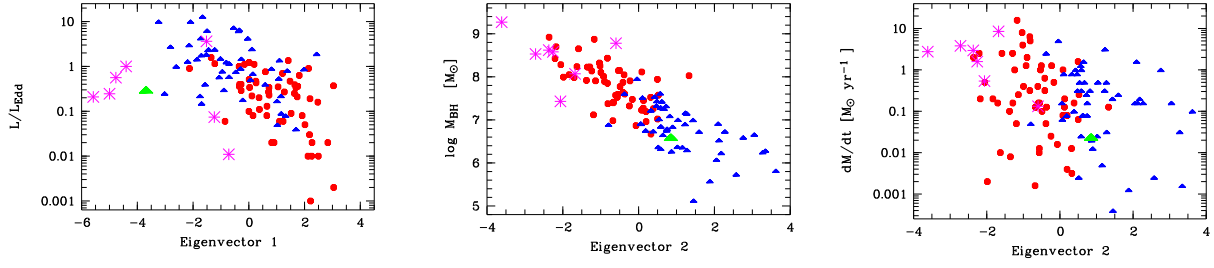


Fig. 5.— Correlations between Eigenvector 1 and L/L_{Edd} , and Eigenvector 2 and black hole mass M_{BH} and the mass accretion rate \dot{M} .

TABLE 1
OBJECT SUMMARY AND CHANDRA OBSERVATION LOG OF THE BAL QSOs

Object Name	RA-2000	Dec-2000	z	D_L ¹	$N_{H,gal}$ ²	E_B-V	TargetID	T-start ³	T-stop ³	MJD	T_{exp} ⁴
SDSS J073733+392037	07 37 33.0	+39 20 37.4	1.7360	12499.4	5.84	0.046	13346	2011-11-14 07:54	2011-11-14 08:54	55879.3500	1539
IRAS 07598+6508	08 04 33.1	+64 59 49.0	0.1483	659.6	4.17	0.047	11850	2010-06-18 08:11	2010-06-18 10:53	55365.3958	6684
PG 0946+301	09 49 41.1	+29 55 19.0	1.2235	8081.1	1.71	0.016	11854	2010-01-11 08:09	2010-01-11 10:30	55207.3889	6518
PG 1001+054	10 04 20.1	+05 13 00.5	0.1611	722.4	1.83	0.014	11852	2010-01-11 06:23	2010-01-11 08:09	55207.3021	1597
PG 1004+130	10 07 26.1	+12 48 56.1	0.2406	1132.1	3.56	0.034	05606	2005-01-05 16:55	2005-01-06 04:37	53375.9479	41064
PG 1115+080	11 18 16.9	+07 45 58.2	1.7355	12494.9	3.57	0.036	11857	2010-02-01 01:57	2010-02-01 06:40	55228.1806	14582
Mkn 231	12 56 14.2	+56 52 25.2	0.0422	174.3	0.96	0.008	11851	2010-07-11 01:51	2010-07-11 03:52	55388.1188	4782
IRAS 14026+4341	14 04 38.8	+43 27 07.4	0.3233	1591.4	1.15	0.010	11855	2010-07-28 14:41	2010-07-28 16:56	55405.6583	6684
SDSS 1437-0147	14 37 48.3	-01 47 10.7	1.311	8809.6	3.21	0.039	11851	2010-07-11 01:51	2010-07-11 03:52	55388.1194	4782
PG 1700+518	17 01 24.8	+51 49 20.0	0.2920	1413.8	2.26	0.030	11853	2010-06-26 19:51	2010-06-26 22:26	55373.8819	6684
PG 2112+059	21 14 52.6	+06 07 42.5	0.466	2454.5	6.09	0.080	03011	2002-09-01 06:35	2002-09-01 23:45	52518.6528	56868

¹The luminosity distance D_L was determined using the cosmology calculator by Wright (2006) assuming a Hubble constant $H_0 = 75 \text{ km s}^{-1} \text{ Mpc}^{-1}$ and is given in units of Mpc

²Galactic Column density by Kalberla et al. (2005) given in units of 10^{20} cm^{-2} .

³Exposure time given in s

⁴Start and end times are given in UT

TABLE 2
Swift OBSERVATION LOG OF THE BAL QSOs

Object Name	ObsID	Segment	T-start ¹	T-stop ¹	MJD	T _{XRT} ²	T _V ²	T _B ²	T _U ²	T _{UVW1} ²	T _{UVM2} ²	T _{UVW2} ²
SDSS J073733+392037	39544	001	2011-08-29 09:41	2011-08-22 22:39	55795.6319	3311	3294	...
		002	2012-01-15 03:45	2012-01-15 03:50	55941.1576	235	254
		003	2012-03-22 05:10	2012-03-22 05:20	56008.2188	584	582
IRAS 07598+6508	80519	001	2013-10-29 21:07	2013-10-29 23:01	56594.9132	2093	84	84	81	169	1296	338
PG 0946+301	08523	001	2013-11-09 23:05	2013-11-09 23:32	56605.9708	1606	131	131	131	261	397	522
		002	2013-11-10 00:41	2013-11-10 00:58	56606.0347	1014	85	85	85	171	227	342
PG 1001+054	80521	001	2013-06-28 08:26	2013-06-28 10:22	56471.3889	1591	...	95	95	1256	...	247
PG 1004+130	80031	001	2012-10-29 08:12	2012-10-29 10:04	56229.3805	1975	1966
		33077	2014-01-10 00:36	2014-01-10 08:34	56667.1910	1838	156	156	156	312	442	626
PG 1115+080	90073	008	2010-02-19 10:19	2010-02-20 15:42	55247.0729	18832	1650	...	1305
		010	2010-03-26 02:32	2010-03-26 23:36	55281.5431	19102	1569	...	1335
		33106	2014-01-17 16:30	2014-01-14 18:22	56674.7257	2168	179	179	179	358	487	718
Mkn 231	32530	001	2012-08-26 04:45	2012-08-26 11:29	56165.3368	2303	2291
		80091	2013-05-09 13:02	2013-05-09 13:21	56421.5500	1124	1121
		32530	2014-01-10 19:53	2014-01-10 21:43	56667.8667	2437	202	202	202	404	556	810
IRAS 14026+4341	80520	001	2013-11-10 21:54	2013-11-10 23:43	56606.9493	1868	87	87	87	175	1072	351
SDSS 1437-0147	91050	001	2012-03-08 09:14	2012-03-08 12:28	55994.4521	250	251	...
		002	2012-03-08 09:16	2012-03-08 12:37	55994.4556	1481	284
		33097	2014-01-18 12:22	2014-01-18 14:06	56675.5521	1029	35	158	158	315	103	215
PG 1700+518	37605	003	2014-01-22 12:14	2014-01-22 12:31	56679.5153	1006	83	83	84	168	231	336
		001	2008-07-06 12:19	2008-07-07 20:35	54654.1875	7364	626	626	626	1253	1603	2506
		002	2008-07-08 02:28	2008-07-08 09:14	54655.2438	2892	347	347	347	694	622	1389
PG 2112+059	80179 33320	001	2012-09-22 21:18	2012-09-22 21:36	56192.8916	1064	1063
		001	2014-06-19 14:31	2014-06-19 19:25	56827.7069	1284	120	1140
		002	2014-06-21 00:24	2014-06-21 00:30	56829.0188	331	326
		003	2014-06-25 04:55	2014-06-25 21:20	56833.5472	1638	1634
		004	2014-07-01 14:44	2014-07-01 16:28	55379.6493	747	735
		005	2014-07-03 07:48	2014-07-03 07:58	56841.3285	587	48	48	48	97	130	194
		006	2014-07-08 22:34	2014-07-08 22:37	56846.9410	152	...	19	43	85

¹Start and end times are given in UT

²Observing time given in s

TABLE 3
2MASS AND WISE FLUXES¹

Object Name	J	2MASS H	K	W1	W2	WISE W3	W4
SDSS J073733+392037	0.319±0.012	0.240±0.013	0.173±0.011	0.176±0.004	0.241±0.005	0.433±0.010	0.476±0.024
IRAS 07598+6508	2.496±0.075	3.731±0.094	6.182±0.109	7.378±0.158	8.086±0.143	5.873±0.076	6.071±0.090
PG 0946+301	0.341±0.013	0.257±0.012	0.219±0.009	0.265±0.006	0.410±0.008	0.394±0.010	0.302±0.016
PG 1001+054	0.362±0.017	0.393±0.014	0.527±0.016	0.807±0.017	0.837±0.016	0.633±0.012	0.540±0.021
PG 1004+130	0.806±0.023	0.635±0.025	0.673±0.020	0.715±0.015	0.765±0.014	0.955±0.016	1.121±0.038
PG 1115+080	0.259±0.017	0.231±0.017	0.185±0.013	0.213±0.005	0.305±0.006	0.464±0.010	0.478±0.019
Mkn 231	14.880±0.280	20.566±0.346	27.600±0.433	30.110±0.872	33.400±0.747	44.961±0.416	87.351±0.895
IRAS 14026+4341	0.799±0.018	0.865±0.023	1.169±0.021	1.896±0.041	2.149±0.040	2.295±0.034	2.778±0.057
SDSS 1437-0147	0.571±0.017	0.519±0.019	0.356±0.013	0.393±0.008	0.635±0.012	0.697±0.012	0.657±0.021
PG 1700+518	1.140±0.024	1.159±0.035	1.490±0.027	2.124±0.044	2.341±0.041	2.249±0.027	2.592±0.046
PG 2112+059	0.571±0.019	0.543±0.016	0.666±0.019	1.034±0.022	1.268±0.024	0.976±0.015	1.063±0.031

¹The fluxes are given in units of 10^{-14} W m⁻², or 10^{-11} erg s⁻¹ cm⁻².

TABLE 4
ANALYSIS OF THE CHANDRA DATA

Object Name	MJD	Model ¹	α_X	$N_{H,z}$ ²	f_{pc}	$F_{0.3-10\text{keV}}$ ³	α_{ox}	$\alpha_{ox,expected}$ ⁴	$\Delta\alpha_{ox}$
SDSS J073733+392037	55879.3500	powl	$0.80^{+0.42}_{-0.41}$	—	—	4.33 ± 0.80	1.80 ± 0.07	1.66	+0.14
IRAS 07598+6508	55365.3958	powl	$1.37^{+0.91}_{-0.68}$	—	—	4.45 ± 1.21	2.34 ± 0.10	1.47	+0.87
PG 0946+301	55207.3889	zwa	$1.09^{+0.98}_{-0.86}$	$13.06^{+9.15}_{-6.96}$	—	3.15 ± 0.25	1.63 ± 0.35	1.59	+0.04
PG 1001+054	55207.3021	powl	$0.86^{+1.03}_{-0.99}$	—	—	0.24 ± 0.13	2.20 ± 0.17	1.40	+0.80
PG 1004+130	53375.9479	zpcfabs	0.50 ± 0.21	$1.15^{+0.66}_{-0.72}$	$0.64^{+0.10}_{-0.14}$	6.63 ± 0.15	1.86 ± 0.06	1.49	+0.37
PG 1115+080	55228.1806	zpcfabs	$1.35^{+0.40}_{-0.38}$	$10.65^{+4.57}_{-4.16}$	$0.92^{+0.05}_{-0.06}$	7.27 ± 0.50	1.42 ± 0.10	1.61	-0.19
Mkn 231	55388.1188	zpcfabs	1.00 (fix)	$4.75^{+3.23}_{-1.68}$	$0.90^{+0.03}_{-0.04}$	17.23 ± 1.84	1.49 ± 0.06	1.26	+0.23
IRAS 14026+4341	55405.6583	powl	1.00 (fix)	—	—	$0.06^{+0.035}_{-0.02}$	2.23 ± 0.37	1.50	+0.73
SDSS 1437-0147	55388.1194	powl	$0.68^{+0.32}_{-0.30}$	—	—	12.11 ± 0.17	1.72 ± 0.07	1.65	+0.07
PG 1700+518	55373.8819	powl	$0.89^{+1.10}_{-0.92}$	—	—	0.15 ± 0.01	2.42 ± 0.12	1.52	+0.90
PG 2112+059	52518.6528	zpcfabs	0.75 ± 0.32	$5.83^{+1.75}_{-1.62}$	$0.82^{+0.08}_{-0.13}$	2.04 ± 0.10	1.78 ± 0.05	1.57	+0.21

¹Models: powl = power law model; zwa = absorption at the redshift of the source with power law continuum; zpcfabs = partial covering absorber model with power law continuum

²Absorption Column density at the redshift of the source given in units of 10^{22} cm^{-2} .

³The absorption corrected 0.3-10 keV flux in the observed frame is given in units of $10^{-16} \text{ W m}^{-1}$, $10^{-13} \text{ erg s}^{-1} \text{ cm}^{-2}$.

⁴Calculated using the relation given in Grupe et al. (2010) and the rest-frame k-corrected luminosity density at 2500Å as listed in Table 5.

⁵The flux was determined from the ACIS-S count rate of $(7.2^{+3.7}_{-2.8}) \times 10^{-4} \text{ counts s}^{-1}$ assuming a power law model with $\alpha_X=1.0$ and Galactic absorption.

TABLE 5
FLUXES OF THE BAL QSOs FROM THE *Swift* OBSERVATIONS

Object Name	ObsID	Segment	MJD	$F_{0.3-10\text{keV}}^1$	F_V^2	F_B^2	F_U^2	F_{UVW1}^2	F_{UVM2}^2	F_{UVW2}^2	α_{UV}	$I_{2500\text{\AA}}^3$
SDSS J073733+392037	39544	001	55795.6319	3.11 ± 0.72	0.45 ± 0.02	...	—	7.24
		002	55941.1576		
		003	56008.2188	5.63 ± 1.35^4	0.94 ± 0.04	0.26 ± 0.02		
IRAS 07598+6508 PG 0946+301	80519	001	56594.9132	$<1.03^5$	3.35 ± 0.13	3.84 ± 0.12	4.43 ± 0.22	3.49 ± 0.20	3.31 ± 0.10	2.51 ± 0.12	0.39 ± 0.01	0.154
	08523	001	56605.9708	$1.9^{+1.9}_-1.0$	0.45 ± 0.04	0.53 ± 0.02	0.53 ± 0.03	0.42 ± 0.03	0.33 ± 0.02	0.22 ± 0.01	0.61 ± 0.22	1.95
PG 1001+054 PG 1004+130	80521	002	56606.0347	...	0.49 ± 0.04	0.58 ± 0.03	0.50 ± 0.03	0.40 ± 0.03	0.35 ± 0.02	0.22 ± 0.02		
	80521	001	56471.3889	$<2.24^5$...	0.66 ± 0.04	0.82 ± 0.05	0.82 ± 0.04	...	0.91 ± 0.05	0.65 ± 0.12	0.040
PG 1004+130	80031	001	56229.3805	$1.91^{+0.95}_-0.71$	1.47 ± 0.06	0.68 ± 0.20	0.245
	33077	001	56667.1910	$2.41^{+1.09}_-0.48$	1.43 ± 0.06	1.92 ± 0.06	2.25 ± 0.09	1.90 ± 0.11	2.08 ± 0.07	1.58 ± 0.07		
PG 1115+080	90073	008	55247.0729	3.70 ± 0.61	0.91 ± 0.05	...	0.64 ± 0.03	-0.15 ± 0.06	2.63
	33106	010	55281.5431	4.17 ± 0.58	0.90 ± 0.05	...	0.64 ± 0.03		
Mkn 231	32530	001	56674.7257	5.83 ± 1.01	0.62 ± 0.03	0.81 ± 0.03	1.04 ± 0.05	0.66 ± 0.04	...	0.51 ± 0.03	2.4×10^{-3}	0.309
	32530	001	56165.3368	8.60 ± 2.13	0.57 ± 0.03		
SDSS 1437-0147	80091	001	56421.5500	$6.85^{+2.70}_-2.23$	0.50 ± 0.02	1.25 ± 0.36	0.309
	32530	002	56667.8667	1.70 ± 0.42	7.17 ± 0.17	5.26 ± 0.10	2.32 ± 0.09	0.87 ± 0.08	0.57 ± 0.02	0.51 ± 0.03		
IRAS 14026+4341	80520	001	56606.9493	$<0.98^5$	1.34 ± 0.07	1.47 ± 0.06	1.20 ± 0.06	0.52 ± 0.04	0.29 ± 0.01	0.19 ± 0.01	0.43 ± 0.09	5.01
	91050	001	55994.4521	$10.48^{+6.73}_-2.42^4$	1.74 ± 0.07	...		
PG 1700+518	33097	002	55994.4556	$16.21^{+4.45}_-2.60$	1.03 ± 0.10	1.23 ± 0.05	1.53 ± 0.07	1.59 ± 0.09	1.74 ± 0.09	1.15 ± 0.07	1.08 ± 0.12	0.457
	37605	003	56679.5153	$0.45^{+0.18}_-0.14$	1.18 ± 0.07	1.40 ± 0.06	1.66 ± 0.08	1.67 ± 0.10	1.58 ± 0.07	1.16 ± 0.06		
PG 2112+059	80179	001	54654.1875	$<0.75^5$	2.22 ± 0.06	2.48 ± 0.06	2.54 ± 0.06	2.11 ± 0.07	2.21 ± 0.08	1.40 ± 0.06	0.07	0.08
	33320	002	54655.2438	$<2.01^5$	2.13 ± 0.06	2.45 ± 0.06	2.40 ± 0.09	1.75 ± 0.06	2.21 ± 0.07	1.17 ± 0.05		
PG 2112+059	33320	001	56192.8916	$2.7^{+1.5}_-1.2$	1.87 ± 0.09	1.88 ± 0.10	0.89 ± 0.10	0.08
	33320	002	56827.7069	$<19.2^5$	2.04 ± 0.10		
PG 2112+059	33320	003	56829.0188	$<3.0^5$	2.00 ± 0.09	0.08	0.06
	33320	004	56833.5472	$<6.4^5$	1.90 ± 0.10		
PG 2112+059	33320	005	55379.6493	$<15.7^5$	1.49 ± 0.10	1.81 ± 0.08	1.88 ± 0.11	1.70 ± 0.12	1.92 ± 0.11	1.73 ± 0.13	0.08	0.06
	33320	006	56841.3285	1.97 ± 0.12	2.04 ± 0.11	1.85 ± 0.13		
PG 2112+059	33320	006	56846.9410	0.08	0.06
	33320	006	56846.9410		

¹Observed 0.3-10 keV flux corrected for Galactic absorption in units of 10^{-16} W m⁻² or 10^{-13} erg s⁻¹ cm⁻².

²Observed UVOT fluxes corrected for Galactic reddening in units of 10^{-14} W m⁻² or 10^{-11} erg s⁻¹ cm⁻².

³k-corrected rest-frame luminosity density at 2500Å in units of 10^{24} W Hz⁻¹ or 10^{31} erg s⁻¹ Hz⁻¹

⁴Spectral analysis from merged dataset

⁵ 3σ upper limits determent using Bayesian statistics as described in Kraft et al. (1991). The count rate was converted into flux using WPIMMS and the spectral parameters obtained from the *Chandra* observation listed in Table 4.

⁶The count rate was converted into flux using WPIMMS and the spectral parameters obtained from the *Chandra* observation listed in Table 4.

⁷Only 152s exposure, not enough to get meaningful upper limits.

TABLE 6
BLACK HOLE MASSES AND L/L_{Edd}

Object Name	FW(H β) ¹	FW(MgII) ¹	$\log L_{5100\text{\AA}}$ ²	$\log L_{3000\text{\AA}}$ ²	$\log M_{\text{BH}}$ ³	$\log L_{\text{Edd}}$ ²	$\log L_{\text{bol}}$ ⁴	$\log L/L_{\text{Edd}}$	FW([OIII]) ¹	$\log([\text{OIII}]/\text{H}\beta)$	$\log(\text{FeII}/\text{H}\beta)$ ⁵
SDSS J073733+392037	—	8470	—	2.51	9.98	4.07	4.20	+0.12	—	—	—
IRAS 07598+6508	3400	—	1.20	—	8.58	2.68	2.00	−0.68	1050	−1.31	+0.42
PG 0946+301	—	4180	—	2.35	9.28	3.38	2.49	−0.89	—	—	—
PG 1001+054	1500	—	0.54	—	7.43	1.53	1.53	+0.00	1200	−0.94	−0.03
PG 1004+130	8300	—	1.25	—	9.27	3.37	2.24	−1.13	1100	−0.63	−0.42
PG 1115+080	—	4215	—	2.40	9.31	3.41	4.39	+0.96	—	—	—
Mkn 231	6530	—	0.47	—	8.78	2.88	0.92	−1.96	980	−0.93	+0.32
IRAS 14026+4341	2880	—	1.58	—	8.62	2.72	2.27	−0.61	530	−2.35	+0.28
SDSS 1437-0147	—	4770	—	2.42	9.43	3.53	4.04	+0.51	—	—	—
PG 1700+518	2440	—	1.69	—	8.53	2.63	2.38	−0.25	720	−1.23	−0.01
PG 2112+059	3010	—	1.48	—	8.07	2.17	2.73	+0.56	1200	−0.56	−0.09

¹All Full Width at Half Maximum are given in units of km s^{−1}.

²uminosities are given in units of 10³⁷ W, or 10⁴⁴ erg s^{−1}

³Black hole masses in units of M_{\odot} , determined using the relations given in Vestergaard & Peterson (2006) and Vestergaard & Osmer (2009).

⁴Bolometric Luminosities are given in units of 10³⁷ W, or 10⁴⁴ erg s^{−1} and are determined between rest-frame 1 μ m and 10 keV.

⁵The FeII flux is measured in the blue FeII blend between 4430 to 4700 \AA , same as it has been used in Grupe et al. (2010).

TABLE 7
MEAN, STANDARD DEVIATION, AND MEDIAN OF WHOLE AGN SAMPLE INCLUDING BAL QSOs, NLS1s¹
AND BAL QSOs

Property	Mean	All AGN			Mean	SD ²	NLS1s		Mean	SD ²	BAL QSOs	
		SD ²	Median	# of AGN			Median	# of NLS1s			Median	# of BAL QSOs
α_X	1.327	0.509	1.250	123	1.661	0.470	1.590	54	0.936	0.266	0.890	11
α_{UV}	0.869	0.772	0.690	122	0.878	0.762	0.690	54	0.963	1.070	0.665	10
α_{ox}	1.385	0.247	1.340	123	1.386	0.228	1.400	54	1.899	0.345	1.800	11
$\Delta\alpha_{ox}$	0.031	0.211	0.009	119	0.059	0.201	0.009	52	0.379	0.381	0.230	11
$\log FWHM(H\beta)^3$	3.365	0.263	3.382	119	3.124	0.120	3.161	54	3.539	0.253	3.491	7
$\log FWHM([OIII])^3$	2.608	0.259	2.607	119	2.610	0.264	2.574	54	2.971	0.132	3.021	7
$\log [OIII]/H\beta$	-0.439	0.513	-0.482	119	-0.507	0.498	-0.569	54	-1.136	0.603	-0.940	7
$\log FeII/H\beta$	-0.178	0.323	-0.161	119	-0.001	0.264	-0.023	54	+0.067	0.292	-0.010	7
$\log M_{BH}^4$	7.458	0.846	7.430	123	6.805	0.559	6.844	54	8.844	0.710	8.780	11
$\log L/L_{Edd}$	-0.473	0.778	-0.366	123	-0.014	0.613	0.000	54	-0.306	0.854	-0.250	11
$\log \dot{M}^5$	-0.649	1.057	-0.700	123	-0.878	0.933	-0.800	54	+0.854	1.116	+0.580	11

¹NLS1s means that we made a cut simply at 2000 km s⁻¹.

²Standard deviation SD

³FWHM are measured in km s⁻¹

⁴Black hole masses are given in units of solar masses, M_{sun} .

⁵The mass accretion rate \dot{M} is given in units of solar masses per year.

TABLE 8
RESULTS FROM THE PRINCIPAL COMPONENT ANALYSIS OF THE WHOLE SAMPLE INCLUDING THE
LOW-REDSHIFT BAL QSOs (118 AGN IN TOTAL).

Property	EV 1	EV 2	EV 3	EV 4	EV 5	EV 6	EV 7	EV 8
Proportion of Variance	0.3787	0.2296	0.1240	0.1034	0.07336	0.05541	0.03116	0.00445
Cumulative Proportion	0.3787	0.6083	0.7322	0.8356	0.90898	0.96439	0.99555	1.00000
α_X	-0.2732	0.4948	0.2886	-0.0355	0.2338	-0.6158	0.4022	0.0174
α_{UV}	0.1994	0.2282	-0.8319	0.1878	0.0179	-0.3804	-0.1182	-0.1482
α_{OX}	-0.4958	-0.2918	-0.0266	0.2369	0.2309	0.0369	0.0167	-0.7465
$\Delta \alpha_{OX}$	-0.4615	-0.2024	-0.1780	0.4637	0.3057	0.0362	-0.0454	0.6344
$\log \text{FWHM}(\text{H}\beta)$	0.2254	-0.6027	-0.1643	-0.1103	0.0054	-0.1854	0.7128	0.0652
$\log \text{FWHM}([\text{OIII}])$	-0.3070	-0.1361	-0.2423	-0.8145	0.3149	-0.0666	-0.2284	0.0963
$\log [\text{OIII}]/\text{H}\beta$	0.4000	0.2054	-0.0049	0.0407	0.7904	0.3798	0.1511	-0.0663
$\log \text{FeII}/\text{H}\beta$	-0.3489	0.3912	-0.3265	-0.1227	-0.2728	0.5389	0.4886	0.0048

A. Additional soft X-ray selected AGN

In addition to the *Swift* observations of the 92 AGN already published in Grupe et al. (2010) we added the remaining AGN in the bright ROSAT AGN sample in Grupe et al. (2001); Grupe (2004) to our sample. These observations were performed by *Swift* after publishing the initial sample of 92 objects (Grupe et al. 2010). These AGN are listed in Table 9. This table contains the coordinated, redshift, $H\beta$ and [OIII] line widths, black hole masses, Eddington ratios, [OIII]/ $H\beta$ and FeII/ $H\beta$ flux ratios, and α_X , α_{UV} and α_{ox} spectral slopes. A description of the *Swift* observations of these additional AGN will be published in a separate paper. Note that this table also contains the information on WPVS 007.

TABLE 9
LIST OF ADDITIONAL BRIGHT SOFT X-RAY SELECTED AGN OBSERVED BY *Swift*

Object Name	RA-2000	Dec-2000	z	FW(H β) ¹	FW([OIII]) ¹	log([OIII]/H β)	log(FeII/H β) ²	log M_{BH} ³	log L/L_{Edd}	α_{X}	α_{UV}	α_{OX}
WPVS 007	00 39 15.2	-51 17 02	0.029	1620	320	-0.74	+0.20	6.60	-0.52	2.65 ⁴	0.82 ⁴	1.89 ⁴
IRAS 01267-2157	01 29 10.7	-21 41 57	0.039	2530	360	-0.50	-0.22	7.64	-0.47	1.24	-0.02	1.33
H 0439-271	04 41 22.5	-27 08 20	0.084	2550	340	+0.29	-0.60	7.58	-0.43	1.00	+2.31	1.04
1 ES 0614-584	06 15 49.6	-58 26 06	0.057	1080	200	-0.89	+0.00	6.23	+0.79	2.19	+1.45	1.24
RX J1019.0+3752	10 19 00.5	+37 52 41	0.135	6200	800	-0.19	-0.46	8.23	-1.30	0.74	+1.10	1.09
RX J1034.6+3938	10 34 38.6	+39 38 28	0.044	700	340	+0.22	+0.14	5.82	+0.87	2.74	+1.83	1.29
PG 1115+407	11 18 30.4	+40 25 55	0.154	1740	340	-1.00	-0.14	7.52	+0.07	1.45	+0.45	1.43
Z 1136+3412	11 39 13.9	+33 55 51	0.033	1450	190	-0.52	+0.01	6.27	-0.30	1.39	+0.17	1.24
Was 26	11 41 16.2	+21 56 21	0.063	2200	220	+0.58	-0.22	7.26	-0.33	1.08	+0.70	1.32
Mkn 1310	12 01 14.4	-03 40 41	0.019	3000	150	+0.11	-0.21	6.67	-1.52	0.85	+1.91	1.15
Mkn 771	12 32 03.6	+20 09 30	0.064	3200	210	-0.55	-0.38	7.40	-0.57	1.12	+0.79	1.38
CBS 150	12 33 41.7	+31 01 03	0.290	1350	460	-0.60	-0.09	7.36	+0.95	1.58	+0.42	1.50
IRAS 12397+3333	12 42 10.6	+33 17 03	0.044	1640	510	+0.27	+0.25	6.66	+0.28	1.47	+3.50	0.83
PG 1244+026	12 46 35.2	+02 22 09	0.049	830	330	-0.06	+0.11	6.07	+0.82	1.75	+0.78	1.31
PG 1322+659	13 23 49.5	+65 41 48	0.168	3100	130	-1.00	-0.37	8.16	-0.40	1.70	+0.43	1.54
QSO 1421-0013	14 24 03.6	-00 26 58	0.151	1500	630	-0.85	-0.16	7.26	+0.63	2.16	+0.47	1.52
SBS 1527+564	15 29 07.5	+56 16 07	0.100	2760	200	+0.52	-0.16	7.15	-0.38	0.82	+0.65	1.33
ESO 404-G029	22 07 45.0	-32 35 01	0.063	6100	280	-0.26	-0.38	8.10	-2.00	0.77	+2.06	1.18
NGC 7214	22 09 07.6	-27 48 36	0.023	4700	530	-0.24	-0.06	7.54	-1.70	0.93	+1.57	1.26
PKS 2227-399	22 30 40.3	-39 42 52	0.318	3710	380	+0.56	-0.41	7.37	-0.05	0.69	+0.03	1.24

¹All Full Width at Half Maximum are given in units of km s⁻¹.

²The FeII flux is measured in the blue FeII blend between 4430 to 4700Å,same as it has been used in Grupe et al. (2010).

³Black hole masses in units of M_{\odot} , determined using the relations given in Vestergaard & Peterson (2006) and Vestergaard & Osmer (2009).

⁴Based on the *Swift* observation of WPVS 007 on 2009-September-17 as reported in Grupe et al. (2013).